NASA-CR-200282

FINAL REPORT : NCC2-5017

Aeroacoustics of Turbulent High-Speed Jets

by

Ram Mohan Rao

and

Thomas S. Lundgren, P.I.

Department of Aerospace Engineering and Mechanics

University of Minnesota, Minneapolis, MN 55455

March 1996

Overview

The objective of this research is to study aeroacoustic noise generation in a supersonic round jet. In particular we want to understand the effect of turbulence structure on the noise without numerically compromising the turbulence itself. This means that direct numerical simulations are needed. In order to use DNS at high enough Reynolds numbers to get sufficient turbulence structure we have decided to solve the temporal jet problem, using periodicity in the direction of the jet axis. Physically this means that turbulent structures in the jet are repeated in successive downstream cells instead of being gradually modified downstream into a jet plume. Therefore in order to answer some questions about the turbulence we will partially compromise the overall structure of the jet.

This report will be presented in two chapters. The first chapter is divided into two sections. The first section describes some work on the linear stability of a supersonic round jet and the implications of this for the jet noise problem. In the second section we will present preliminary work done using a TVD numerical scheme on the CM5 at the University of Minnesota. This work is only two-dimensional (plane) but shows very interesting results, including weak shock waves. However this is a non-viscous computation and the method resolves the shocks by adding extra numerical dissipation where the gradients are large. One wonders whether the extra dissipation would influence small turbulent structures like small intense vortices. Nevertheless we are still pursuing a three-dimensional version using this method for the purpose of comparing with other methods, and perhaps answering some of our doubts.

The second chapter is an extensive discussion of preliminary numerical work using the spectral method which we prefer to use to solve the compressible Navier-Stokes equations to study turbulent jet flows. The method uses Fourier expansions in the azimuthal and streamwise direction and a 1-D B-spline basis representation in the radial direction. The B-spline basis is locally supported and this ensures block diagonal matrix equations which are solved in O(N) steps. A very accurate highly resolved direct numerical simulation (DNS) of a turbulent jet flow is expected. This is a modification of a boundary layer code developed by Bob Moser.

Chapter 1 : Preliminary Studies of Inviscid Compressible Jets

Section 1 : The stability of a supersonic round jet

Our purpose in doing this stability problem is to provide initial conditions for the nonlinear computations. We want to start with the most unstable disturbance since this is what would be found in the natural problem. This problem has been studied by Tam and Hu(1989) however they didn't present the information which we require. As a result of our computations we have found some new results which have not been previously reported.

The basic stability equation was obtained by linearizing the equations for inviscid compressible flow in cylindrical coordinates, taking small perturbations from an axially symmetric basic state. One can reduce this to a single second order equation for the pressure perturbation, which is expressed in separation of variables form as

$$p = \bar{p}(r) + \hat{p}(r)e^{(i\omega t - ikz - im\theta)}$$

where r is the radial coordinate. The equation for $\hat{p}$ is

$$\frac{d^2\hat{p}}{dr^2} + \Big(\frac{1}{r} + \frac{2kd\bar{u}/dr}{\omega - \bar{u}k} - \frac{1}{\bar{\rho}}\frac{d\bar{\rho}}{dr}\Big)\frac{d\hat{p}}{dr} + \Big(\frac{(\omega - \bar{u}k)^2}{\bar{a}^2} - k^2 - \frac{m^2}{r^2}\Big)\hat{p} = 0$$

where $\bar{u}(r)$ is the prescribed axial velocity profile, $\bar{p}(r)$ and $\bar{\rho}(r)$ the prescribed pressure and density of the base state, and $\bar{a}^2(= \gamma R\bar{T})$ is the square of the sound speed. This equation agrees with Tam and Hu. This equation is to be solved with boundary conditions which require the solution to be bounded at $r = 0$ and to possess only outgoing waves at infinity. It is an eigenvalue problem for complex ω when k and m are given. The flow is unstable if $\mathrm{Im}\omega < 0$.

The velocity profile was taken in the same form as in Tam and Hu as a "half-Gaussian" function which is given by

$$\bar{u} = u_j \qquad r < h$$

$$\bar{u} = u_j \exp\Big(-\ln 2\big(\frac{r-h}{b}\big)^2\Big) \qquad r > h$$

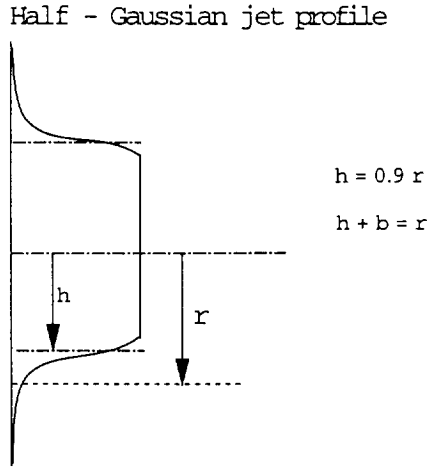

which is sketched here in order to define the parameters b and h. We define the jet radius to be $r_j = b + h$ and all computations were done with $b/r_j = .1, h/r_j = .9$. We have taken the temperature profile to be of a form similar to the velocity

$$\bar{T} = T_j \quad r < h$$

$$\bar{T} = T_\infty + (T_j - T_\infty) \exp\Big(- \ln 2 \big(\frac{r-h}{b}\big)^2 \Big) \quad r > h$$

and have taken $\bar{p}(r) = p_\infty$, constant across the jet. Then $\bar{\rho}$ is related to $\bar{T}$ by

$$p_\infty = \bar{\rho} R \bar{T}$$

and

$$\bar{a}^2 = a_\infty^2 \bar{T}/T_\infty.$$

Sometimes in problems like this the temperature is related to the velocity profile by the Crocco-Buseman formula. But this is a viscous dominated profile which results when the Prandtl number is unity, and it doesnt make a lot of sense for high Reynolds number flows such as this. In all the work done by us so far we have taken $T_j = T_\infty$ so the temperature is constant across the jet.

We have solved this eigenvalue problem by a method described in a book by Betchov and Criminale. We integrate inward from a large radius, using an asymptotic formula to identify outgoing waves, and we integrate outward from the origin. Where the two computations meet we must have $\hat{p}$ and $d\hat{p}/dr$ continuous. This does not occur unless

ω has the proper value. We iterate on ω using a Newton-Raphson procedure until our continuity requirement is attained. The biggest problem was that the procedure doesn't converge unless one starts near the proper value. This means that is was necessary to change parameters by small increments, starting from a known result.

Results have been obtained for jet Mach numbers of $M_j = 2$ and 2.5. The result for $M_j = 2$ is shown in a figure at the end of this section. Here we present curves of growth rate versus k for a number of values of m (the azimuthal wavenumber). What is observed is that the maximum growth rate for given m increases as m increases, reaching a maximum at $m = 4$ and then it decreases again as m becomes greater that 4. This means that of all azimuthal wavenumbers the most unstable wave is $m = 4$ (and also $m = -4$ since only m^2 occurs in the equation). For $M_j = 2.5$ the maximum is at $m = \pm 5$.

A wave $\exp(-ikz - im\theta)$ is interpreted as a helical wave on the surface of the jet, with the wave making an angle $\tan^{-1}(m/k)$ with the axis of the jet ($m = 0$ is an axial wave). Therefore there are two helical waves of definite angle, one left-handed and one right-handed, which are the most unstable. This is similar to results of Sandham and Reynolds (1990) on the stability of a compressible mixing layer. They find two oblique waves with maximum growth rate which make equal but opposite angles with the flow direction.

There are some implications of this for our proposed nonlinear computation. Sandham and Reynolds (1991) in a second paper find a single oblique unstable plane wave rolls up into an oblique vortex. We expect that a single unstable helical wave will roll up into a helical vortex. Since our helical waves propagate downstream with a speed which is about .66 times the jet speed, we expect a similar speed for the helical vortex. A propagating helix will appear like a rotating helix–as a barber pole does. This is an interesting result because there are observed jet modes, called spinning modes, where the noise field rotates around the jet axis, so that to an observer on one side the sound appears to have a time periodicity(Wesley and Woolley, 1975).

Sandham and Reynolds found that the angle of the most unstable oblique wave depends on the convective Mach number in such a way that $M_c \cos\alpha \simeq .6$, so that the

component of the Mach number perpendicular to the wave stays constant (and subsonic). We find approximately the same result for the helical waves, based on only two Mach numbers. In the Sandham-Reynolds nonlinear computations they find that because the normal Mach number is subsonic the oblique vortex forms without shock waves (unlike their strictly two-dimensional computations which do have shocks). This is possibly very significant for our proposed computations. It means that helical vortices could form without shocks. This is important when we use the B-spline/spectral method because any shocks will have to be resolved by viscosity alone which could restrict our Reynolds number range.

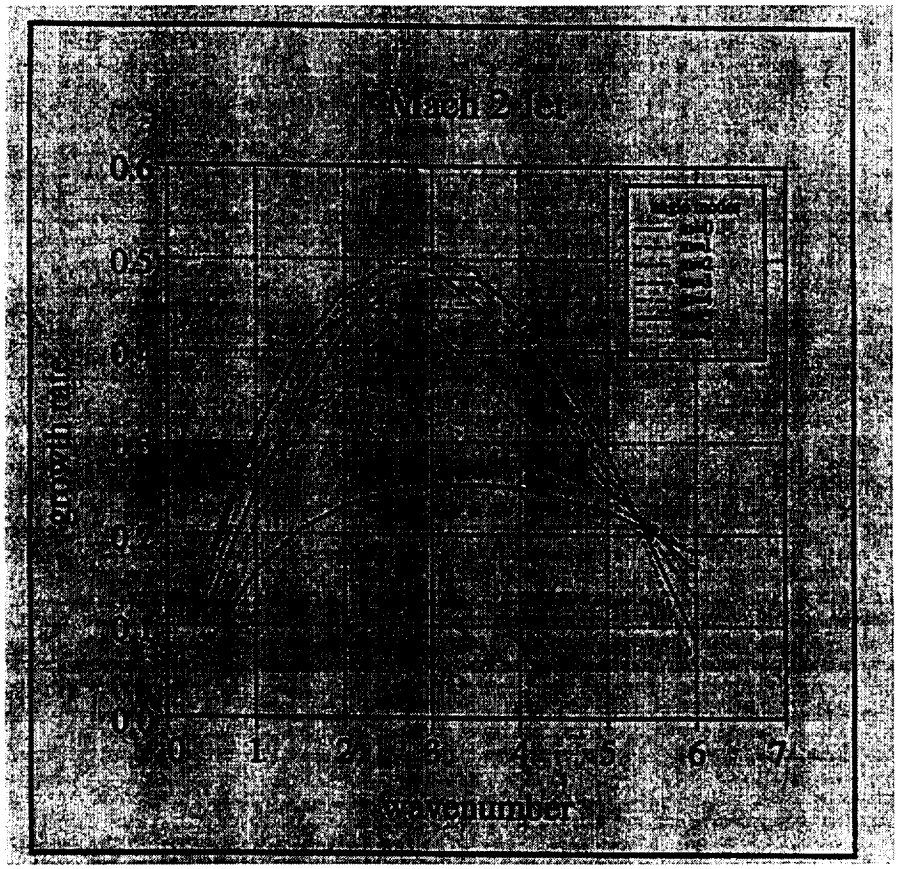

Section 2 : A Study of 2-D, Unsteady, Inviscid, Compressible Jets Using a Second Order TVD Scheme

Computations of a two-dimensional supersonic temporal jet were made as a preliminary study of the non-reflecting boundary conditions and to gain some experience with the temporal jet configuration. This was done using an efficient, parallel TVD [5-7] scheme in a data-parallel environment to run on massively parallel processing (MPP) computers. All the calculations are carried out on Thinking Machines' CM-5. It is hoped that these calculations will help discern the intricacies of 2-D compressible jet flows. An attempt is made to resolve the turbulent scales(vortex structures) using very fine meshes. No turbulence model is used. Since these are inviscid calculations the numerical dissipation of the scheme is used to approximate viscous dissipation effects of real fluids. In this study a second order explicit non-MUSCL upwind TVD algorithm as proposed by Yee [7] is used.

Initially a 2-D version of the half-gaussian jet profile described in the previous section is used. Anti-symmetric disturbances were imposed on the initial jet profile since they were found to be more unstable. This ensures the break down of the shear layer into small vortical structures.

The computational domain was discretized into a very fine mesh of 512*512 grid cells. The physical dimensions of the domain are twice the wavelength of the most unstable wave (found from linear stability analysis) in the streamwise direction and 3 to 4 jet diameters in the transverse direction. Grid stretching is used for a layer of cells (one jet diameter wide) near the boundary in order to weaken any outgoing waves. At the transverse boundaries the approximate non-reflecting boundary condition [10] $p' \pm \rho a v' = 0$ was used. The primed quantities are perturbations from mean flow, and a is the speed of sound.

Simulations for a fully expanded cold jet at centerline Mach number of 2.0 are presented.

Highly resolved flow solutions capturing a wide range of turbulent scales are achieved. Figures 1-3 show the various stages of temporal jet development. The Mach contour and pressure contours show distinct development of shocks which were absent initially. The isobars also show alternating high and low pressure regions corresponding to vortical

structures. From the vorticity contours we notice that the initial structure of two vortex sheets breaks down into smaller vortices.

It is evident from the plots that the non-reflecting conditions work fairly well.

Figures

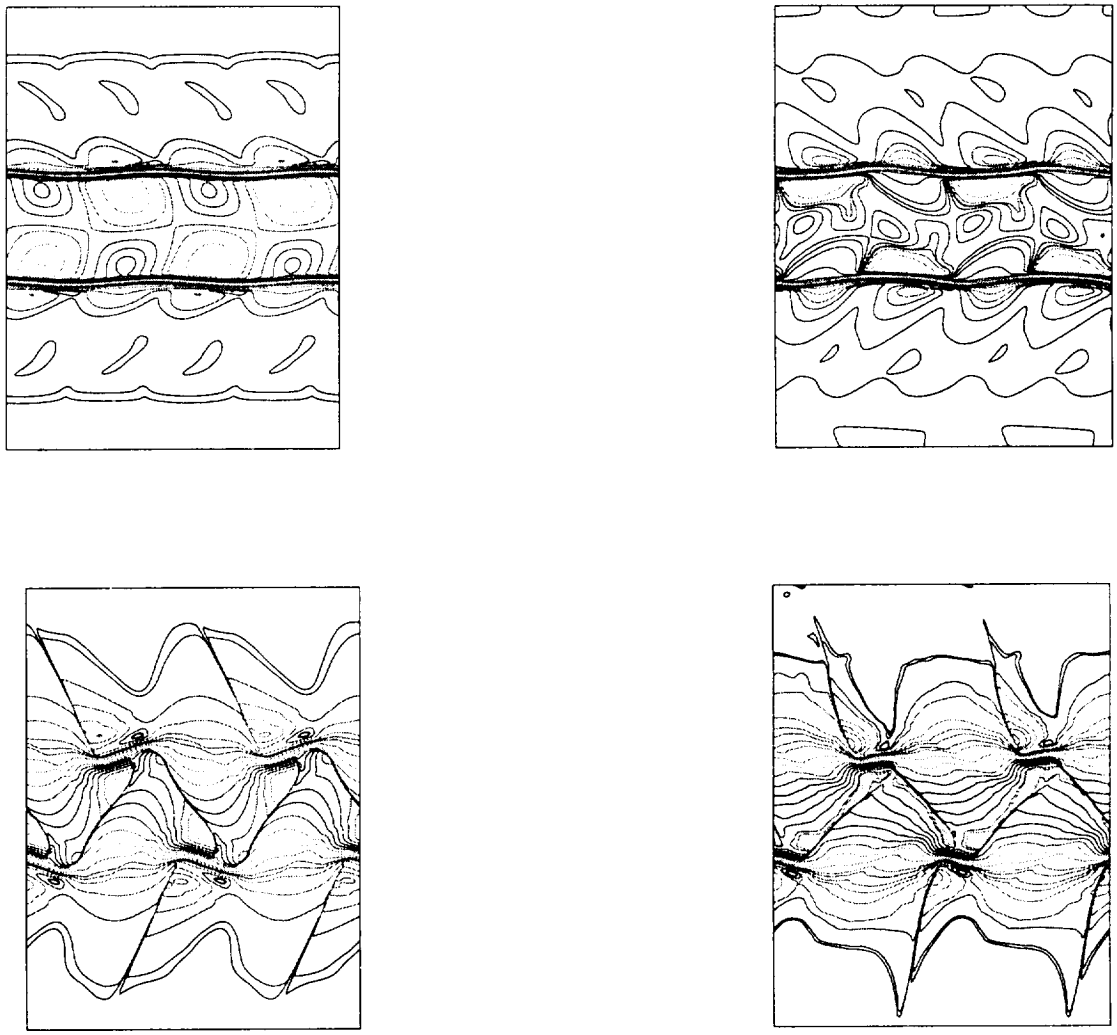

Fig. 1 Contour plots of Mach Number after 1000,1900,4000, and 7300 time steps

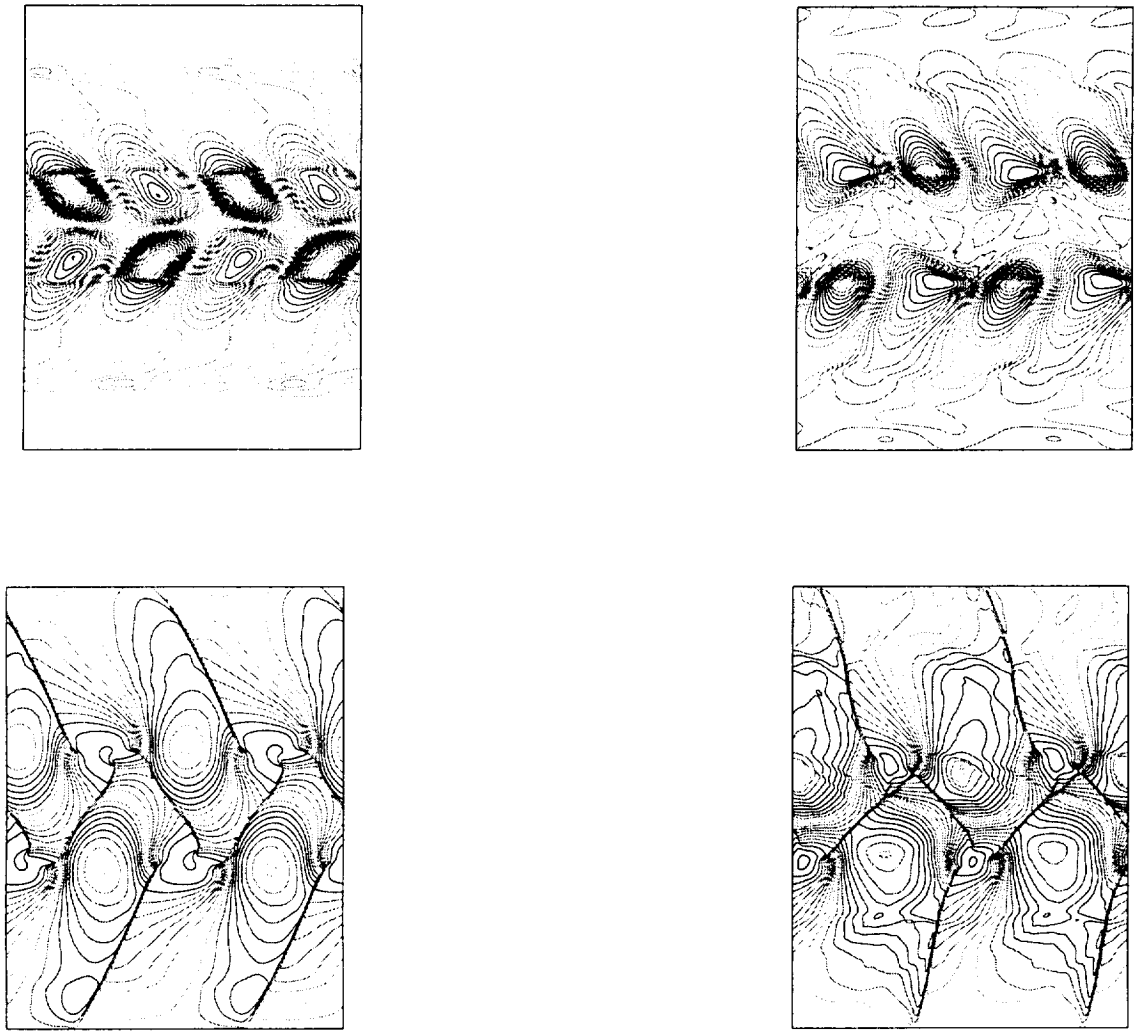

Fig. 2 Contour plots of Pressure after 1000, 1900, 4000, and 7300 time steps

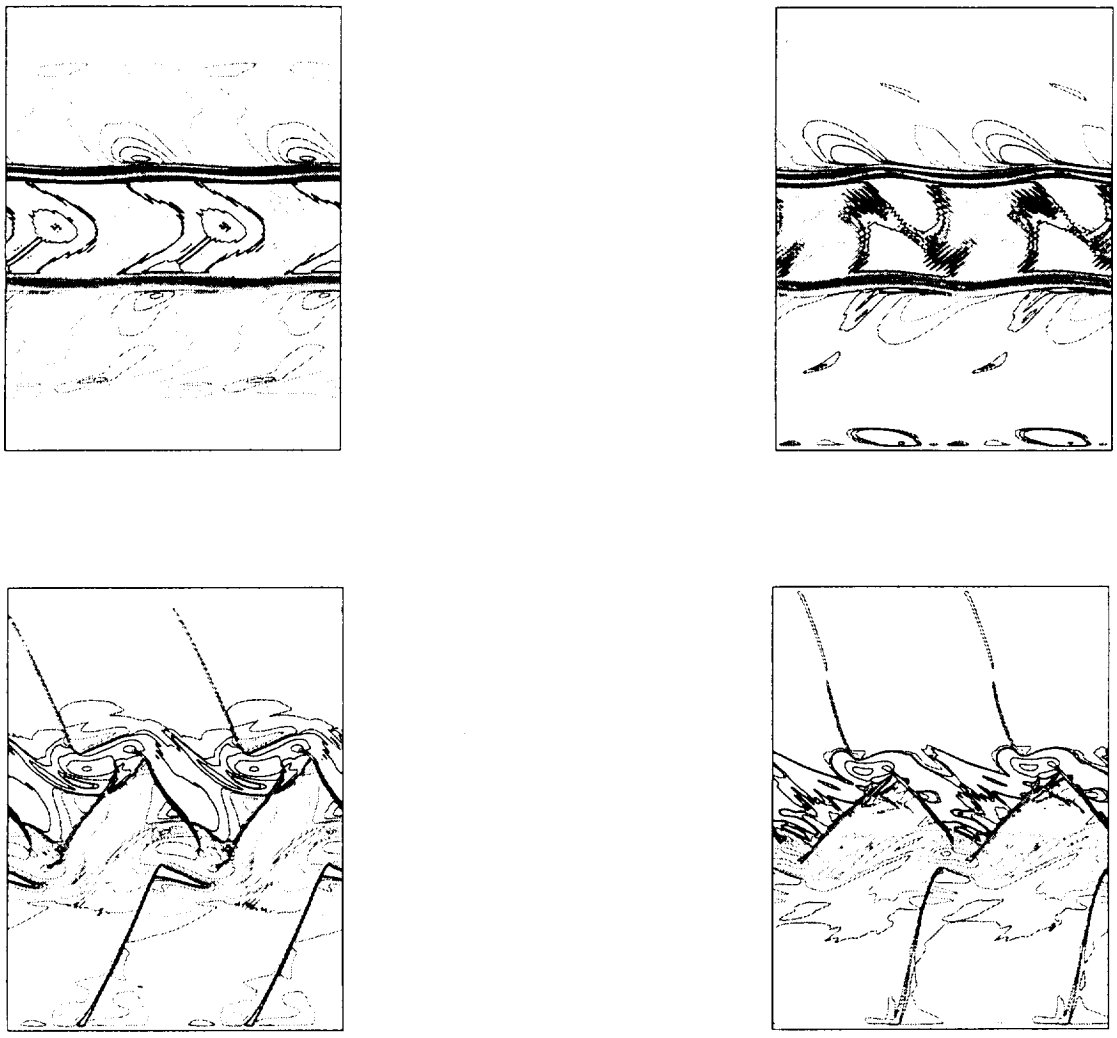

Fig. 3 Contour plots of Vorticity after 1000, 1900, 4000, and 7300 time steps

References for Chapter 1

[1] Sandham, N. D., & Reynolds, W. C., " Compressible mixing layer: linear theory and direct simulation ", AIAA *Journal*, **28**, 1990, pp. 618–624.

[2] Sandham, N. D., & Reynolds, W. C., " Three-dimensional simulations of large eddies in the compressible mixing layer ", *J. Fluid Mech.*, **224**, 1991, pp. 133–158.

[3] Tam, C. K. W., and Hu, F. Q., " On the three families of instability waves of high speed jets ", *J. Fluid Mech.* **201**, 1989, pp. 447–483.

[4] Westley, R., and Woolley, J. H., " Sound pressures of a choked jet oscillating in the spinning mode ", Presented as Paper 75-479 at the AIAA 2nd Aero-Acoustics Conference, Hampton, Va. 1975.

[5] Yee, H. C., Warming, R. F., and Harten, A., " Implicit Total Variation Diminishing (TVD) Schemes for Steady-State Calculations ", *J. Comp. Phys.*, **57**, 1985, pp. 327-360.

[6] Harten, A., " On a Class of high Resolution Total–Variation–Stable Finite Difference Schemes ", *SIAM J. Num. Anal.*, **21**,1984, pp.-23.

[7] Yee, H. C., " A Class of High Resolution Explicit and Implicit Shock –Capturing Methods ", NASA TM-101088, February 1989.

[8] Thinking Machines Corp. " CM-5 Technical Summary ", 1993.

[9] Soetrisno, M, Eberhardt, S., Riley, J. J., and McMurtry, P., " A Study of Inviscid, Supersonic Mixing Layers Using a Second-Order Total Variation Diminishing Scheme," AIAA *Journal*, **12**, 1989, pp. 1170 -1778.

[10] Giles, M. B., " Non-reflecting Boundary Conditions for Euler Equation Calculations ", AIAA *Journal*, **28**, 1990, pp. 2050-2058.

[11] Colonious, T., Lele, S. K., Moin, P., " Boundary Conditions for Direct Computations of Aerodynamic Sound Generation ", AIAA *Journal*, **31**(9), 1993, pp. 1574-1582.

Chapter 2 : Direct Numerical Simulation of Unsteady, Compressible Round Jets

Introduction

Jet noise is a major concern in the design of a supersonic transport (SST) aircraft. Studies by various researchers[2-4] lead to aerodynamic noise as a major contributor to jet noise. Some of these studies indicate that most of the aerodynamic jet noise due to turbulent mixing occurs when there is a rapid variation in turbulent structure, i.e. rapidly growing or decaying vortices.

The object of this work is to obtain highly accurate flow solutions of a turbulent round jet. These solutions are expected to help understand the various turbulent scales and mechanisms of turbulence generation in the evolution of a compressible round jet. We hope to use these accurate flow solutions to estimate acoustic radiation in the near-field region. Also the data generated can be used to compute various turbulence quantities such as mean velocities, turbulent stresses, etc. which may aid in turbulence modeling.

We simulate a compressible round jet by using Fourier expansions in the azimuthal and streamwise direction and a 1-D B-spline basis representation in the radial direction. This is an efficient and accurate way to separate out the θ and z variables, leaving partial differential equations(PDEs) depending on r and t only. By using a 1-D B-spline basis and a Galerkin approximation we can reduce this set of PDEs to ordinary differential equations(ODEs) in time. This is solved by a 3^{rd} order Runge-Kutta time marching scheme. The present study uses a spectral method developed by Moser *et al.*[7]

We consider the temporal jet problem for two reasons: one since this configuration allows for the application of highly accurate spectral methods and the other because the dynamics of the temporal jet is not greatly different from that of a spatially evolving jet. The spectral accuracy helps capture smaller turbulent scales.

Governing Equations

The compressible Navier-Stokes equations written in cylindrical coordinates in non-dimensional form are,

$$\frac{\partial \sigma}{\partial t} = \sigma^2 \Big(\frac{1}{r}\frac{\partial (r m_r)}{\partial r} + \frac{1}{r}\frac{\partial m_\theta}{\partial \theta} + \frac{\partial m_z}{\partial z} \Big) \tag{1}$$

$$\begin{aligned}
\frac{\partial m_r}{\partial t} + \frac{\sigma}{r}(m_r^2 - m_\theta^2) &= -\frac{\partial \sigma m_r m_k}{\partial x_k} - \frac{\partial P}{\partial r} + \frac{1}{Re}\Big(\frac{\partial \tau_{rk}}{\partial x_k} + \frac{\tau_{rr} - \tau_{\theta\theta}}{r} \Big) \\
\frac{\partial m_\theta}{\partial t} + \frac{2\sigma}{r} m_r m_\theta &= -\frac{\partial \sigma m_\theta m_k}{\partial x_k} - \frac{1}{r}\frac{\partial P}{\partial \theta} + \frac{1}{Re}\Big(\frac{\partial \tau_{\theta k}}{\partial x_k} + 2\frac{\tau_{\theta r}}{r} \Big) \\
\frac{\partial m_z}{\partial t} + \frac{\sigma}{r} m_r m_z &= -\frac{\partial \sigma m_z m_k}{\partial x_k} - \frac{\partial P}{\partial z} + \frac{1}{Re}\Big(\frac{\partial \tau_{zk}}{\partial x_k} + \frac{\tau_{zr}}{r} \Big)
\end{aligned} \tag{2}$$

$$\frac{\partial P}{\partial t} + \nabla \cdot P\vec{\mathbf{u}} = -(\gamma - 1) P \nabla \cdot \vec{\mathbf{u}} + \frac{1}{Re\ Pr}\nabla \cdot \vec{q} + \frac{(\gamma - 1)}{Re}\Phi \tag{3}$$

where,

$$\frac{\partial}{\partial x_1} = \frac{\partial}{\partial r}\ , \quad \frac{\partial}{\partial x_2} = \frac{1}{r}\frac{\partial}{\partial \theta}\ , \quad \frac{\partial}{\partial x_3} = \frac{\partial}{\partial z}$$

$\sigma = \frac{1}{\rho}$, $m_k = \rho\ u_k$, $Re = \frac{\rho u l}{\mu}$, $Pr = \frac{\mu C_p}{\kappa}$

Re, Pr are the Reynolds number and Prandtl number, C_p is the specific heat at constant pressure, and Φ is the viscous dissipation (see Appendix).

B-Spline Representation and Galerkin Formulation

The flow variables are expanded using Fourier sums in the two periodic directions, *viz.* the azimuthal (θ) and the axial (z) directions. In the non-periodic or radial direction (r) we use 1-Dimensional B-splines as interpolating functions.[1] B-splines have local support and hence lead to sparse block diagonal matrices which can be efficiently stored and solved. Application of boundary conditions is similar in ease to a finite element method (FEM).

B-splines of order n are piecewise polynomials of degree n having $n - 1$ continuous derivatives. Since they have a high degree of continuity derivatives of quantities (like velocity to get vorticity) can be smoothly and accurately represented.

They have 1 degree of freedom(d.o.f) per interval unlike finite element(FE) basis which can have as many d.o.f as the order of the polynomial. We use B-spline bases because higher order FE bases may resolve waves of wavelength smaller than twice the interval

length due to the increased d.o.f. But this is beyond the Nyquist cut-off for the interval size and so these increased d.o.f do not improve the resolution (i.e. the smallest accurately represented scale) of the solution only thing that gets better is the accuracy (convergence rate is increased). Higher order B-splines on the other hand not only have better accuracy but also have better resolution of scales per d.o.f.

The Galerkin method using B-splines as basis functions has been used previously by some researchers.[5-7] By using a Galerkin approximation we can approximate the set of PDEs as a set of ODEs in time.

One can use a B-spline basis to represent the desired function $f(x)$ as,

$$f(x) = \sum_{j=-\infty}^{\infty} a_j \; b_j^n(x) \tag{4}$$

where,

$b_j^n(x)$ is a n^{th} order B-spline coefficient, a_j is the value of function at knot j.

Using a Galerkin approximation we can write, (b_k is the weight function)

$$\int b_k \; f(x)dx = \sum_j a_j \int b_j b_k dx \tag{5}$$

Also, the derivative of $f(x)$ can be written as,

$$f'(x) = \sum_j a_j \; b_j'(x) \tag{6}$$

But here the order of the polynomial has reduced by 1 so in order to keep the degree of polynomial the same we approximate the derivative as,

$$f'(x) \approx g(x) \;\Rightarrow\; \sum_j a_j \; b_j'(x) \;\approx\; \sum_j c_j^n \; b_j^n(x) \tag{7}$$

Again the Galerkin approximation is written as,

$$\int b_k \; f'(x)dx \approx \sum_j a_j \int b_j' \; b_k dx \tag{8}$$

Any non-linear terms are handled in a similar way, i.e. if

$$h = f \cdot g$$

$$h = \sum_j d_j \; b_j^n(x) \;\approx\; \sum_{j,k} a_j \; c_k \; b_j \; b_k$$

$$\sum_j d_j \int \; b_j \; b_l \; dx \;\approx\; \sum_{j,k} a_j \; c_k \int b_j \; b_k \; b_l \; dx \tag{9}$$

The matrices (terms with the integral) on the right hand side of equations (5) and (8) are called the mass and derivative matrices respectively. All different combinations of such derivatives and other terms are computed as matrices too. These are calculated only once using a Gaussian quadrature and stored as opposed to a regular finite element (FE) basis where they can be calculated on the fly when required.

Writing the governing equations in the Galerkin form using the B-spline representation yields a number of matrices similar to the mass and derivative matrices, non-linear advection terms yield matrices similar to the non-linear matrix obtained in equation (9).

In Galerkin form the continuity equation can be written for any k_θ and k_z as (k_θ and k_z are wave numbers in the θ and z directions respectively),

$$\begin{aligned} \frac{\partial}{\partial t} \sigma_i \sum_l \int_R b_i \; b_l \; r dr \;=\; & \sum_{j,\;k,\;l} \sigma_i \sigma_j \Big(m_{r_k} \int_R \frac{b_i \; b_j \; (r \; b_k)' \; b_l}{r} \; r dr \\ & + \frac{\partial}{\partial \theta} m_{\theta_k} \int_R \frac{b_i \; b_j \; b_k \; b_l}{r} \; r dr \;+\; \frac{\partial}{\partial z} m_{z_k} \int_R b_i \; b_j \; b_k \; b_l \; r dr \Big) \end{aligned} \tag{10}$$

where,

$$\sigma \;=\; \sum_k \sigma_k(z,\theta,t) \; b_k(r) \;, \qquad m_\theta \;=\; \sum_k m_{\theta_k}(z,\theta,t) \; b_k(r) \;,$$

$$m_r \;=\; \sum_k m_{r_k}(z,\theta,t) \; b_k(r) \;, \qquad m_z \;=\; \sum_k m_{z_k}(z,\theta,t) \; b_k(r)$$

The Fourier terms ($e^{ik_\theta} e^{ik_z}$) are included in the coefficients of the variables. So $\sigma_k(z,\theta,t) = \sigma_k(t) \sum_{k_\theta} \sum_{k_z} e^{ik_\theta \theta + ik_z z}$ and so on.

Since we are using 1-D B-splines all the integrals are line integrals over the radius. These are computed exactly using Gaussian quadratures (doing integrals exactly takes care

of aliasing). The derivatives in the θ and z are taken by Fast Fourier Transforming (FFT) into wave space and multiplying by the appropriate wave numbers k_θ and k_z, and then an inverse FFT is applied to bring it back to physical space.

The momentum and energy equations can be written in a similar manner.

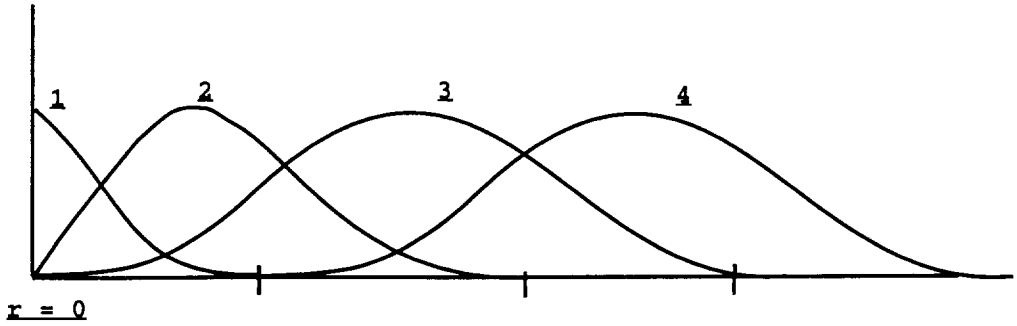

Fig 1 Quadratic B-Splines

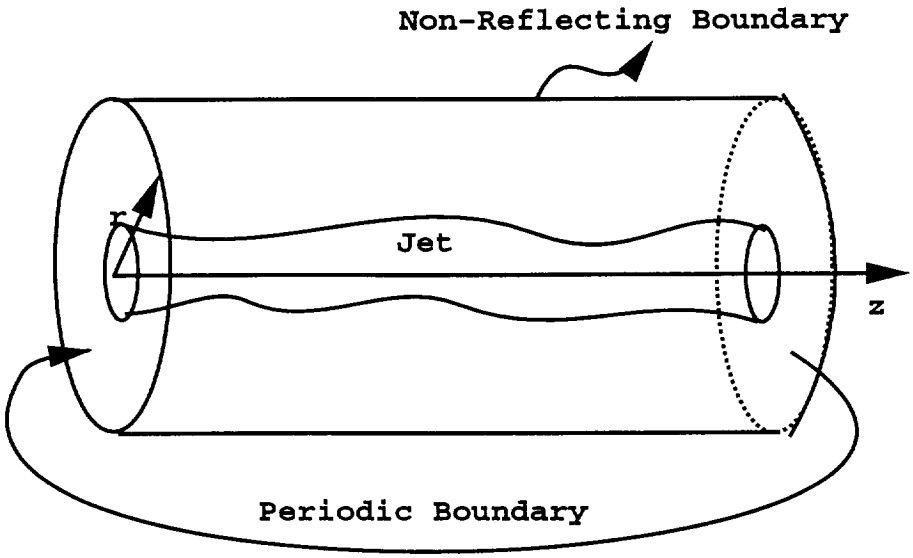

Fig 2 Computational Domain

Numerical Formulation

Writing the flow equations in a manner as discussed above results in a linear system

of coupled equations to solve simultaneously at each time step. Since these B-splines (of order n) have local support on $n+1$ knot(node) intervals (see fig.1) we get a $2n+1$ block banded matrix system.

$$\mathbf{M}\, f \;=\; R \tag{11}$$

where,

$\mathbf{M}$ is the resulting mass matrix, f is the column vector of nodal values we solve for, and R is a column matrix resulting from the RHS of the governing equations.

Time integration is carried out by a 3^{rd} order Runge-Kutta scheme.

Regularity Requirements

In the cylindrical coordinate system the origin ($r = 0$) is source of concern since some of the functions do not remain analytic as they have a 'r' in the denominator. From a mathematical point of view the flow variables should be single valued and finite. To enforce this the polynomial expansion functions must satisfy some regularity requirements.[8]

The z-component of the velocity should be represented as,

$$\begin{aligned} u_z(r;\ m,k) \;&= a(m,k)\ r^{|m|}\ P_z(r^2;\ m,k)\ e^{i\ m\theta}\ e^{i\ kz},\ m = all\ \ integers, \\ P_z(0;\ m,k) &= 1, \end{aligned} \tag{12}$$

where $P_z(r^2;\ m,k)$ is a polynomial in r^2.

Scalars and z-components of all vectors should be represented in a similar manner. The θ and r-components of the vectors are dependent on each other and should be represented as,

$$\begin{aligned} u_r(r;\ m,k) \;&=\; b(m,k)\ r^{|m|-1}\ P_r(r^2;\ m,k)\ e^{i\ m\theta}\ e^{i\ kz}, \\ u_\theta(r;\ m,k) \;&=\; c(m,k)\ r^{|m|-1}\ P_\theta(r^2;\ m,k)\ e^{i\ m\theta}\ e^{i\ kz}, \\ c(m,k) \;&=\; ib(m,k) \quad for\ m\ \geq 1, \\ c(m,k) \;&=\; -ib(m,k) \quad for\ m\ \leq -1, \\ P_r(0;\ m,k) \;&=\; P_\theta(0;\ m,k) = 1, \end{aligned} \tag{13}$$

for $m = 0$ $\quad b(m,k)$ and $c(m,k)$ are unrelated.

Enforcing these conditions gives rise to a set of constraint equations which then replace some rows in the mass matrix and suitably modify the RHS vector R.

We can obtain the constraint equations as follows, for a quadratic B-Spline and any scalar u,

$$u(r;\ m,k)\ =\ a(m,k)\ r^{|m|}\ P(r^2;\ m,k)\ e^{i\ m\theta}\ e^{i\ kz},\ m = all\ \ integers,$$

Only non-zero derivatives allowed are $|m| + 2j \quad \forall\, j \geq 0$

For quadratic B-splines (see fig.1), at $\underline{r = 0}$, 3 splines have support at the origin. Order of non-zero derivatives for the splines is,

$$Spline\ 1 \Rightarrow 0,\ 1,\ 2$$

$$Spline\ 2 \Rightarrow 1,\ 2$$

$$Spline\ 3 \Rightarrow 2$$

All other splines are zero at $r = 0$.

Consider spline expansions as $\sum_i a_i\ b_i$, where b_i are the spline coefficients. We have in any interval,

$$\sum_i b_i = 1 \Rightarrow b_1 + b_2 + b_3 = 1$$

$$b_1' + b_2' = 0 \Rightarrow b_1' = -b_2'$$

Now consider different values of the azimuthal wave number m,

$\underline{\text{for } m = 0}$

Only non-zero derivatives allowed are 0, 2, ... even powers, so all odd powered derivatives should be forced to zero. At $r = 0$ splines having non-zero first derivative are splines 1 and 2, so,

$$a_1 b_1' + a_2 b_2' = 0 \tag{14}$$

for $m = 1$

Only non-zero derivatives allowed are 1, 3, ... odd powers, so all even powered derivatives should be forced to zero. At $r = 0$ splines having non-zero 0^{th} and 2^{nd} derivatives are splines 1 and splines 1, 2, and 3 respectively, giving constraints,

$$\begin{aligned} a_1 &= 0, \; and \\ a_2 b_2'' + a_3 b_3'' &= 0 \end{aligned} \tag{15}$$

Similarly,

for $m = 2$

Only non-zero derivatives allowed are 2, 4, ... even powers, giving

$$a_1 = 0, \quad a_2 = 0 \tag{16}$$

and

for $m = 3$

Only non-zero derivatives allowed are 3, 5, ... odd powers, so

$$a_1 = a_2 = a_3 = 0 \tag{17}$$

or, all splines should be zero. For all other values of m we get the same result as (17). Now equations (14-17) are the **constraint equations** which will replace the appropriate rows in the matrix $\mathbf{M}$ and vector R.

Before replacing rows which actually contain the physics of the flow care has to be taken to see that no information is lost. So, we need to take a linear combination of those rows to be replaced and add them to the remaining rows in a particular manner. For this the null space of the constraint equations has to be computed and the eigenvectors of this space are to be used for the linear combination. This is done as shown below.

for $opol = 7$ and $m = 1$

The first set of rows in the mass matrix are written as,

$$\mathbf{m}' = \begin{pmatrix} 1 & 0 & 0 & 0 & 0 & 0 & 0 \\ * & * & * & * & * & * & * \\ 0 & b_2^2 & b_3^2 & 0 & 0 & 0 & 0 \\ * & * & * & * & * & * & * \\ 0 & b_2^4 & b_3^4 & b_4^4 & b_5^4 & 0 & 0 \\ * & * & * & * & * & * & * \\ 0 & b_2^6 & b_3^6 & b_4^6 & b_5^6 & b_6^6 & b_7^6 \end{pmatrix}$$

The rows with $*$'s are the unconstrained rows and the b_j^i are the bspline derivatives. Now to choose a set of null vectors X_j such that,

$$m' X_j = 0 \tag{18}$$

Let us choose

$$X_j = \begin{pmatrix} 0 & 0 & 0 \\ 1 & 0 & 0 \\ x_{11} & 0 & 0 \\ 0 & 1 & 0 \\ x_{12} & x_{21} & 0 \\ 0 & 0 & 1 \\ x_{13} & x_{22} & x_{31} \end{pmatrix}$$

So we can compute the null vectors using equation 18.

Now the mass matrix $\mathbf{M}$ is modified by using the null vectors for linear combinations as,

$$row_2 = row_2(original) + x_{11} * row_3 + x_{12} * row_5 + x_{13} * row_7$$

$$row_4 = row_4(original) + x_{21} * row_5 + x_{22} * row_7$$

$$row_6 = row_6(original) + x_{31} * row_7$$

This has to be done for all values of the azimuthal wave number m.

This procedure can similarly be applied to all the flow vectors and scalars appearing in the vector f. The derivation of constraints is similar for higher order splines.

CFL and Modal Reduction

Another concern arising due to a cylindrical mesh is that near the origin the aspect ratio of the cells gets very high, so we have to reduce the number of azimuthal modes

near the origin to maintain a good CFL number. This we will call mode suppression. So we effectively reduce the number of azimuthal modes to 1 near the origin and increase it successively such that at the outer boundary we have all the azimuthal modes.

This reduces the accuracy but helps us increase the time-step, dt, by a significant amount. Another advantage of doing this is that the computational domain in Fourier space is significantly smaller thus allowing faster computations. *i.e.* For lower azimuthal wave number x, the computations have to carried out for more radial points, but as x increases fewer radial points have to be considered. Another way to look at it would be near the origin fewer x loops need to be considered.

This is to be implemented by making the upper bound of the x-loops to be dependent on y, *i.e.* x= 1 to nx-modified[y] if the y-loop is the outer loop, or making the lower bound of the y-loop dependent on x if the x-loop is the outer loop, *i.e.* y = ny-min[x] to ny.

Optimizations

The code was optimized thus,

- Moved all major computations (rhs of governing equations) to separate subroutines thus reducing the load on the main program and enabling it to be unrolled and vectorized more efficiently.
- Manually unrolled the quadrature sum loops. This helped in decreasing the number of operations by eliminating a lot of repetitive computations due to proper regrouping. Similar and symmetric matrix multipliers were regrouped together thus reducing redundant calculations.
- Vectorizing over larger loops.

Following the above procedure has helped reduce the time taken per mode per Runge-Kutta step considerably.

Boundary conditions

Ideally, the computational domain should mimic the physical domain by including all free space and only having physical boundaries. But this is not possible and the

computational domain has to be finite. So we need artificial boundaries to limit the computational domain. But we want these artificial boundaries to be invisible to the flow field so that vortices and other waves can pass through these boundaries and leave the domain without giving rise to spurious reflection waves. So we need non-reflecting boundary conditions (NRBCs).

In solving a temporally evolving jet the inflow-outflow boundaries are made periodic (see fig 2). This might not be very accurate but serves the purpose of studying turbulence. Also it takes care of the inflow-outflow boundary conditions. This also enables us to use a spectral expansion in the axial direction. So the only boundaries of concern are the transverse numerical boundaries. If we have good boundary conditions we can make the computational domain smaller and thus get a higher resolution and compute finer scales.

Several investigators [9-14] have studied and used different types of non-reflecting boundary condtions. Engquist and Majda [12,13] study the wave equation and develop a perfectly non-reflecting boundary condition using pseudo-differential operators. But this equation is non-local in both space and time and is of little use for computational purposes as we would have to store data on the boundary from previous time-steps. But by approximating the operator they also develop a hierarchy of approximate NRBCs , with the increasing accuracy in passing obliquely incident waves.

We use the first order non-reflecting boundary conditions for outflow at the transverse boundary, which can also be derived from physical considerations using 1-D Riemann Invariants. The outflow boundary condition is,

$$\frac{\partial}{\partial t}p' - \rho_\infty c_\infty \frac{\partial}{\partial t}u'_r = -\frac{c_\infty}{2\,R}p' \tag{19}$$

where R is radius of outer boundary, and the primed quantities represent the perturbations from mean flow and the ∞ quantities represent free stream or mean flow. The term on the right hand side is a correction for a cylindrical boundary.

This boundary condition is supposed to ensure that there are no incoming waves from infinity. It works well for directly incident waves. We think that this will serve the purpose since we would have nearly cylindrical wavefronts incident on the boundary which is also

cylindrical. In addition we hope to mitigate the outgoing wave amplitudes by coarsening the mesh gradually as we approach the boundary as was done in the 2-D preliminary work.

Now to implement this boundary condition in our scheme we have to transform the last set of equations, which represent the physics at the boundary, to characteristic variables at each substep of the Runge-Kutta algorithm.

This is done using the following transformation matrix from Giles.[9]

$$\begin{pmatrix} c_1 \\ c_2 \\ c_3 \\ c_4 \\ c_5 \end{pmatrix} = \begin{pmatrix} \rho_\infty^2 c_\infty^2 & 0 & 0 & 0 & 1 \\ \rho_\infty^2 c_\infty u_\theta & c_\infty & 0 & 0 & 0 \\ -\rho_\infty^2 c_\infty u_r & 0 & -c_\infty & 0 & 1 \\ \rho_\infty^2 c_\infty u_z & 0 & 0 & c_\infty & 0 \\ \rho_\infty^2 c_\infty u_r & 0 & c_\infty & 0 & 1 \end{pmatrix} \begin{pmatrix} \delta\sigma \\ \delta m_\theta \\ \delta m_r \\ \delta m_z \\ \delta p \end{pmatrix} \tag{20}$$

where the c_i's are the characteristic variables and the δ-quantities are time incremental quantities.

So we can modify the last five rows of the mass matrix and the right-hand-side using the above transformation.

Equation 19 can be written as

$$-\rho_\infty^2 c_\infty u_r \delta\sigma - c_\infty \delta m_r + \delta p = -\frac{c_\infty}{2\,R} p'$$

So to implement the above b.c. we have to replace the third of the last five rows including the right-hand-side by the above equation since the third characteristic c_3 has the right form for the b.c.

Test Cases

A few simple test cases were run to validate the code and for diagnostic purposes. In all cases the desired steady state solutions were obtained to machine accuracy. All cases except the rotating flow case were run using quadratic B-splines.

Case 1 : Uniform flow through a circular pipe

Flow conditions are,

$u_\theta = 0$, $u_r = 0$, $p = \frac{1}{\gamma}$, $\sigma = T$

R = 1

$$u_z = \frac{\kappa Re}{4\mu}(R^2 - r^2)$$

Choose $\kappa = \frac{4\mu}{Re}$ then,

$$u_z = (1 - r^2)$$

From the temperature equation (eqn 5) we have a balance,

heat flux = - viscous dissipation

or,

$$\frac{\mu}{RePr}\nabla^2 T = \frac{\gamma - 1}{Re}\Phi$$

(refer Appendix)

Solving the above equation and applying the b.c's

$$\frac{\partial T}{\partial r}|_{r=0} = 0$$

$$T_{r=R} = 1$$

gives,

$$T = \frac{\gamma - 1}{4} Pr(1 - r^4) + 1$$

This test case helps check the temperature equation and uniform flow in the z - direction.

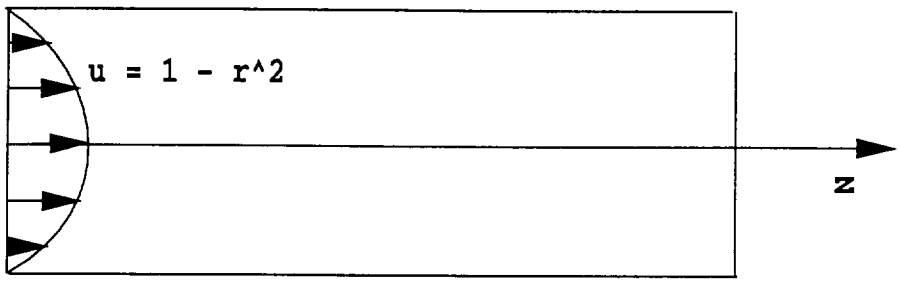

Fig. 3

Case 2 : Uniform flow through permeable boundaries

Flow conditions are, $u_r = ucos\theta$, $u_\theta = -usin\theta$, $u_z = 0$, $p = \frac{1}{\gamma}$, $\sigma = 1$

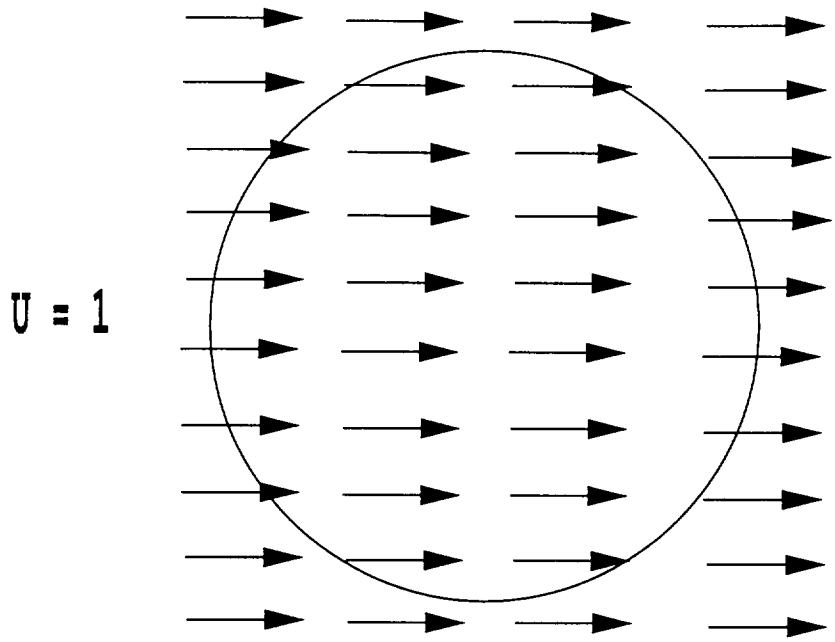

Fig. 4

This checks the flow jacobians and also non-axially symmetric flow.

Case 3 : Uniform Rotating Flow

Flow conditions are,

$u_\theta = r\Omega$, $u_r = 0$, $u_z = 0$, $T = 1$

The momentum equation reduces to,

$$\frac{\partial p}{\partial r} = \frac{\rho u_\theta^2}{r}$$

$$\gamma \sigma p = 1$$

if p at outer radius is p_o,

$$p = p_o e^{\frac{\gamma r^2 \Omega^2}{2}}$$

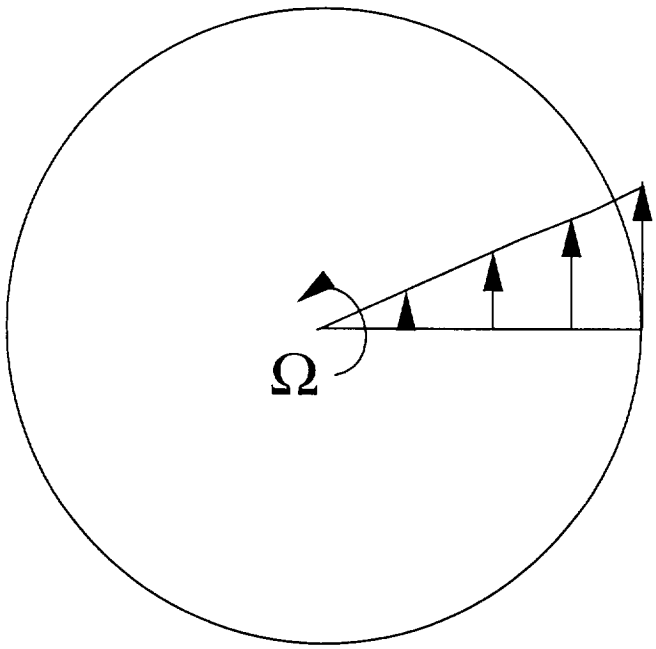

Fig. 5

This flow tests the azimuthal dependence. Here we had to switch to higher order B-splines since the variables are exponential functions and are better represented by higher order B-splines.

Case 4 : Spherically Radiating Flow

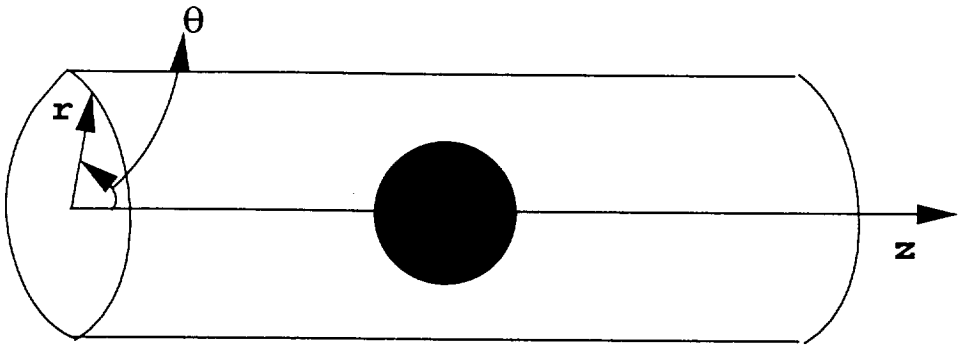

Fig. 6

This is to test the non-reflecting b.c's.

We consider a spherically radiating point source flow placed at the center of a cylindrical domain. The solution is singular at the origin and is therefore picked up after a finite time and is treated as an initial value problem. This test case is very robust, since there exists an exact time-dependent solution with which we can compare our results. This test case not only tests the non-reflecting boundary conditions but also helps validate the entire code.

The radiating bubble is considered as a perturbation to the mean flow which is,

$P = \frac{1}{\gamma}$, $\sigma = 1$, $u_r = u_z = u_\theta = 0$

The perturbation is taken as a point source solution of the linear wave equation which is written as a velocity potential $\Phi = \frac{f(t-\frac{x}{c})}{x}$. Where $x = \sqrt{r^2 + z^2}$, c is sound speed, and t is the time. f can be any function. We have used a cubic function for f,

$$\Phi = \begin{cases} -\frac{1}{4\pi x}(t - \frac{x}{c})^3(t_1 - t + \frac{x}{c})^3 & c(t - t_1) \leq x \leq ct, \\ 0 & otherwise \end{cases}$$

The function is plotted below.

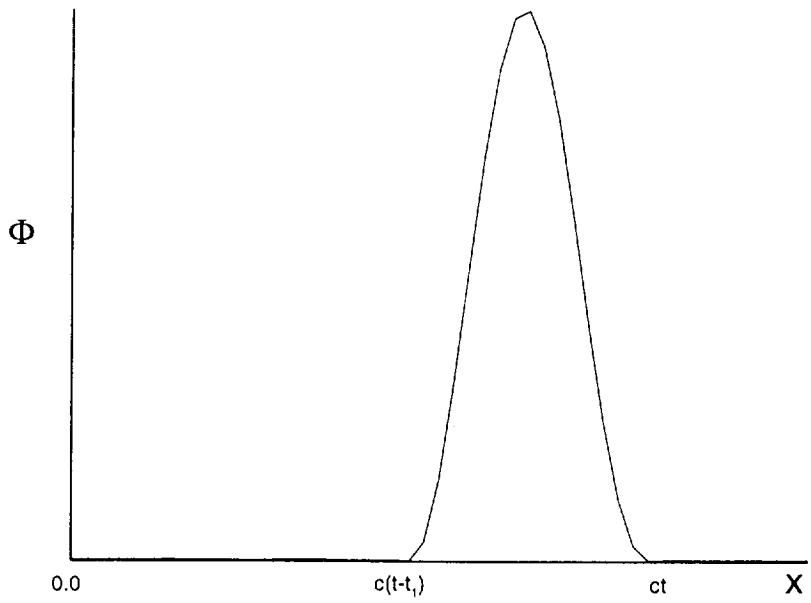

Fig. 7

The fundamental perturbations are expressed in terms of the velocity potential as,

$$p' = -\rho_\infty \frac{\partial \Phi}{\partial t}$$
$$\sigma' = p'$$
$$u'_r = \frac{\partial \Phi}{\partial r}$$
$$u'_\theta = 0$$
$$u'_z = \frac{\partial \Phi}{\partial z}$$

Plotted below are the density profiles as time progresses. The dotted profiles which almost overlap the solid lines are the exact solutions. Figure 8 plots density versus r at $z = 0$, while figure 9 shows density versus z at $r = 0$. Figure 10 shows a cross section

of the spherical wave in a $r - z$ plane. From the plots we can see that the non-reflecting conditions work fairly well. The waves which are incident normally pass through the artificial boundaries with little or no reflection. In figures 8 and 10 the plots with $t = t_3$ show a weak reflected residual wave. This is as expected since the non-reflecting conditions are exact for normally incident waves, but oblique waves would cause some reflection. These reflected wave amplitudes can be further reduced by stretching the grid near the boundary (not done here).

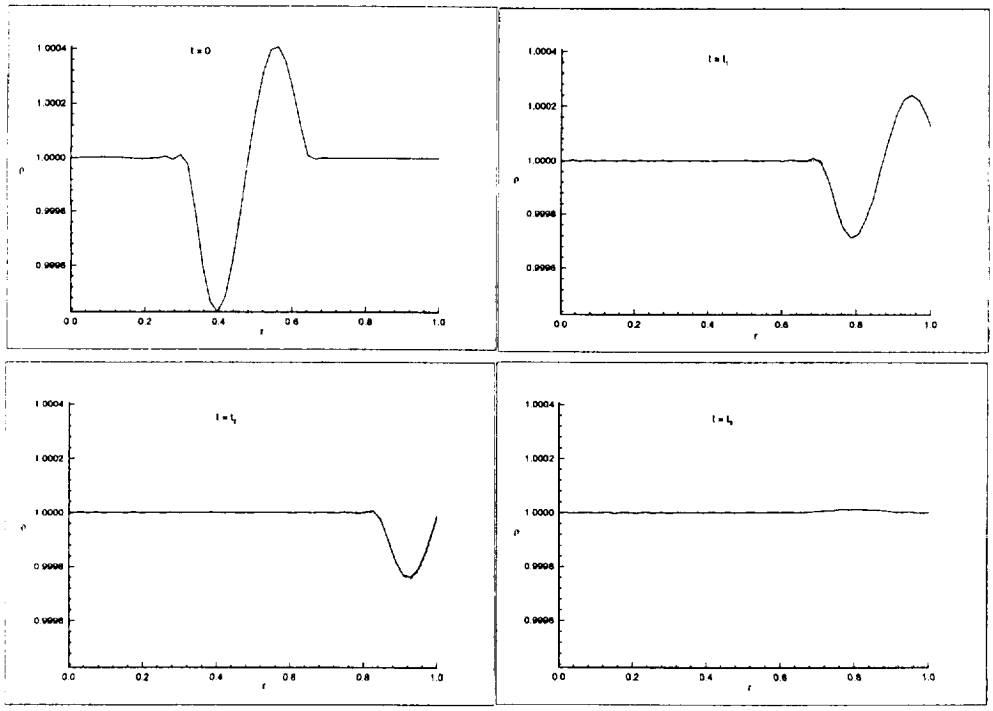

Fig. 8

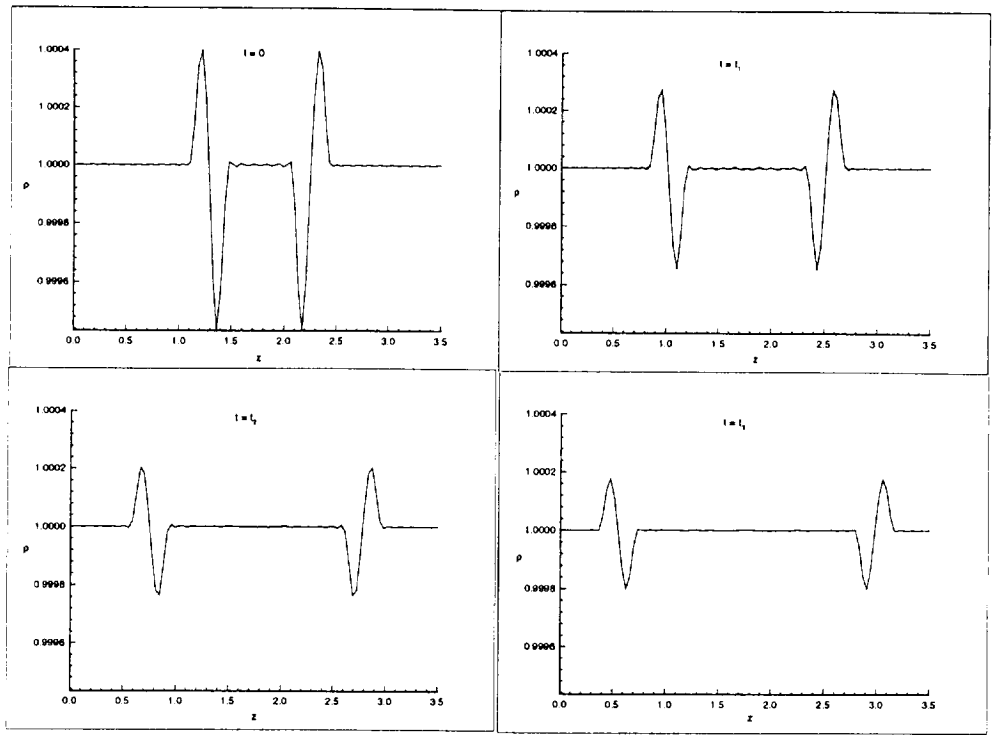

Fig. 9

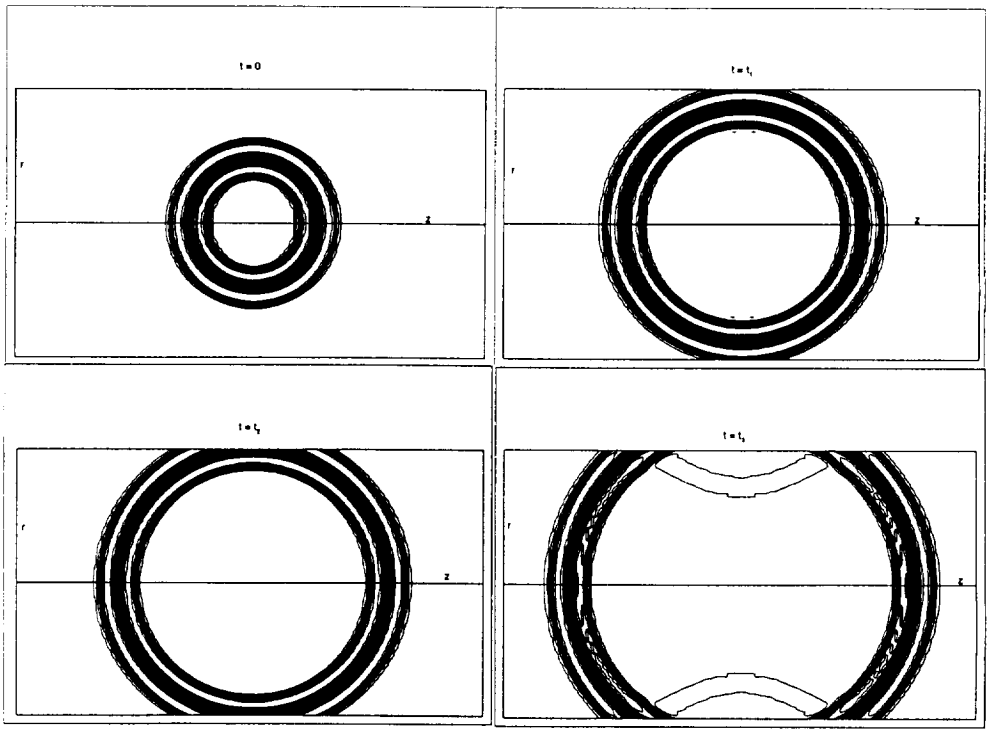

Fig. 10

A more general and similar test case would be to shift the origin of the point source

off the z-axis. So the flow is not axis-symmetric anymore.

Conclusions

A Numerical code based on the spectral method of Moser [7] was developed in cylindrical coordinates using Fourier expansions in the azimuthal and streamwise direction and a 1-D B-spline basis representation in the radial direction. Time integration is carried out by a 3^{rd} order Runge-Kutta time marching scheme.

The code was validated against some test cases. Non-reflecting boundary conditions, used at the outer boundary, have also been satisfactorily tested.

References for Chapter 2

[1] De Boor, C., " *A Practical Guide to Splines* ", Springer-Verlag, 1978.

[2] Tam, C. K. W., and Burton, D. E., "Sound Generated by Instability Waves of Supersonic Jets, Part 1. Two Dimensional Mixing Layers, Part 2. Axissymmetric Jets", *J. Fluid Mech.*, **138**, 1984, pp.249 -271, 273-295.

[3] Tam, C. K. W., " Stochastic Model Theory of Broadband Shock Associated Noise from Supersonic Jets", *Journal of Sound and Vibration*, **116**, 1987, pp.265-302.

[4] Tam, C. K. W., and Tanna, H. K., " Shock Associated Noise from Supersonic Jets from Convergent-Divergent Nozzles", *Journal of Sound and Vibration*, **81**, 1982, pp.337-358.

[5] Gardner, L. R. T., Gardner, G. A., Zaki, S. I., and El Sahhrawi, Z., " B-Spline Finite Element Studies of the Non-Linear Schrodinger Equation". *Computer Methods in Applied Mechanics and Engineering*, **108**, September 1993, pp.303-318.

[6] Kasi Vishwanadham, K. N. S., and Koneru, S. R., " Finite Element Method for One-Dimensional and Two-Dimensional Time Dependent Problems with B-Splines", *Computer Methods in Applied Mechanics and Engineering*, **108**, September 1993, pp.201-222.

[7] Moser, R. D., Moin, P., and Leonard, A., " A Spectral Numerical Method for the Navier-Stokes Equations with Applications to Taylor–Couette Flow ", *J. Comp. Phys.*, **52**, No. 3, December 1983, pp.524-544.

[8] Shariff, K., " Comment on Coordinate Singularities by P. R. Spalart ", Personal Communication.

[9] Giles, M. B., " Non-reflecting Boundary Conditions for Euler Equation Calculations", AIAA *Journal*, **28**, December 1990, pp.2050-2058.

[10] Colonious, T., Lele, S. K., Moin, P., " Boundary Conditions for Direct Computations of Aerodynamic Sound Generation", AIAA *Journal*, **31**, No.9, September 1993, pp.1574-1582.

[11] Poinsot, T. J., and Lele, S. K., " Boundary Conditions for Direct Simulations of

Compressible Viscous Flows ", *J. Comp. Phys.*, **101**(1), 1992, pp. 104-129.

[12] Engquist, B., and Majda, A., " Absorbing Boundary Conditions for the Numerical Simulation of Waves ", *Math. Comput.*, **31**(139), 1977, pp. 629-651.

[13] Engquist, B., and Majda, A., " Radiation Boundary Conditions for Acoustic and Elastic Wave Calculations ", *Commun. Pure Appl. Math.*, **32**, 1979, pp. 313-357.

[14] Givoli, D., " Non-Reflecting Boundary Conditions ", *J. Comp. Phys.*, **94**, 1991, pp. 1-29.

[15] Sandham, N. D., and Reynolds, W. C., " Compressible Mixing Layer : Linear Theory and Direct Simulation ", AIAA *Journal*, **28**, 1989, pp.618 - 624.

[16] Sandham, N. D., and Reynolds, W. C., " Three-Dimensional Simulation of Large Eddies in the Compressible Mixing Layer ", *J. Fluid Mech.*, **224**, 1991, pp.133-158.

Appendix

The compressible Navier-Stokes equations in cylindrical coordinates

$$\frac{\partial \rho}{\partial t} + \frac{1}{r}\frac{\partial (r\rho u_r)}{\partial r} + \frac{1}{r}\frac{\partial (\rho u_\theta)}{\partial \theta} + \frac{\partial (\rho u_z)}{\partial z} = 0 \qquad (A.1)$$

$$\begin{aligned}
\rho\Big(\frac{Du_r}{Dt} - \frac{u_\theta^2}{r}\Big) &= -\frac{\partial P}{\partial r} + \frac{\partial \tau_{rr}}{\partial r} + \frac{1}{r}\frac{\partial \tau_{r\theta}}{\partial \theta} + \frac{\partial \tau_{rz}}{\partial z} + \frac{\tau_{rr} - \tau_{\theta\theta}}{r} \\
\rho\Big(\frac{Du_\theta}{Dt} + \frac{u_r u_\theta}{r}\Big) &= -\frac{1}{r}\frac{\partial P}{\partial \theta} + \frac{\partial \tau_{\theta r}}{\partial r} + \frac{1}{r}\frac{\partial \tau_{\theta\theta}}{\partial \theta} + \frac{\partial \tau_{\theta z}}{\partial z} + 2\frac{\tau_{r\theta}}{r} \\
\rho\frac{Du_z}{Dt} &= -\frac{\partial P}{\partial z} + \frac{\partial \tau_{zr}}{\partial r} + \frac{1}{r}\frac{\partial \tau_{z\theta}}{\partial \theta} + \frac{\partial \tau_{zz}}{\partial z} + \frac{\tau_{zr}}{r}
\end{aligned} \qquad (A.2)$$

where,

$$\tau = \mu \begin{pmatrix} 2\big(\frac{\partial u_r}{\partial r} - \frac{1}{3}\nabla\cdot\vec{\mathbf{u}}\big) & \frac{1}{r}\frac{\partial u_r}{\partial \theta} + r\frac{\partial}{\partial r}\big(\frac{u_\theta}{r}\big) & \frac{\partial u_z}{\partial r} + \frac{\partial u_r}{\partial z} \\ \frac{1}{r}\frac{\partial u_r}{\partial \theta} + r\frac{\partial}{\partial r}\big(\frac{u_\theta}{r}\big) & 2\big(\frac{1}{r}\frac{\partial u_\theta}{\partial \theta} + \frac{u_r}{r} - \frac{1}{3}\nabla\cdot\vec{\mathbf{u}}\big) & \frac{\partial u_\theta}{\partial z} + \frac{1}{r}\frac{\partial u_z}{\partial \theta} \\ \frac{\partial u_z}{\partial r} + \frac{\partial u_r}{\partial z} & \frac{\partial u_\theta}{\partial z} + \frac{1}{r}\frac{\partial u_z}{\partial \theta} & 2\big(\frac{\partial u_z}{\partial z} - \frac{1}{3}\nabla\cdot\vec{\mathbf{u}}\big) \end{pmatrix}$$

$$\begin{aligned}
\frac{D}{Dt} &= \frac{\partial}{\partial t} + u_r\frac{\partial}{\partial r} + \frac{u_\theta}{r}\frac{\partial}{\partial \theta} + u_z\frac{\partial}{\partial z} \\
\nabla\cdot\vec{\mathbf{u}} &= \frac{1}{r}\frac{\partial r u_r}{\partial r} + \frac{1}{r}\frac{\partial u_\theta}{\partial \theta} + \frac{\partial u_z}{\partial z}
\end{aligned}$$

μ is the viscosity,

$$\frac{\partial P}{\partial t} + \nabla\cdot P\vec{\mathbf{u}} = -(\gamma-1)P\nabla\cdot\vec{\mathbf{u}} + (\gamma-1)\nabla\cdot\vec{q} + (\gamma-1)\Phi \qquad (A.3)$$

$\vec{q}$ is the heat flux, T is the temperature, κ is heat conductivity,

$$\vec{q} = -\kappa\nabla T, \qquad T = \gamma\ \sigma\ P$$

and Φ is viscous dissipation given by,

$$\begin{aligned}
\Phi =& \mu\Big(2\Big(\big(\frac{\partial u_r}{\partial r}\big)^2 + \big(\frac{1}{r}\frac{\partial u_\theta}{\partial \theta} + \frac{u_r}{r}\big)^2 + \big(\frac{\partial u_z}{\partial z}\big)^2\Big) \\
&+ \big(\frac{1}{r}\frac{\partial u_z}{\partial \theta} + \frac{\partial u_\theta}{\partial z}\big)^2 + \big(\frac{\partial u_r}{\partial z} + \frac{\partial u_z}{\partial r}\big)^2 + \big(\frac{1}{r}\frac{\partial u_r}{\partial \theta} + \frac{\partial u_\theta}{\partial r} - \frac{u_\theta}{r}\big)^2 - \frac{2}{3}(\nabla\cdot\vec{\mathbf{u}})^2\Big)
\end{aligned}$$

Acknowledgements

This work was supported in part by the Army Research Office contract number DAALO 3-89-C-0038 with the University of Minnesota Army High Performance Computing Research Center (AHPCRC) and the DoD Shared Resource Center at the AHPCRC. This work is supported by a NASA Ames grant NASA/NCC2 - 5017. We also acknowledge the support of the Minnesota Supercomputer Institute.